Magnon gap mediated lattice thermal conductivity in $MnBi_2Te_4$

Dung D. Vu [1], Ryan A. Nelson [4], Brandi L. Wooten [3], Joseph Barker [5], Joshua E. Goldberger [4], and Joseph P. Heremans [1,2,3,*]

[1]*Department of Mechanical and Aerospace Engineering, The Ohio State University, Columbus, Ohio 43210, USA*
[2]*Department of Physics, The Ohio State University, Columbus, Ohio 43210, USA*
[3]*Department of Materials Science and Engineering, The Ohio State University, Columbus, Ohio 43210, USA*
[4]*Department of Chemistry and Biochemistry, The Ohio State University, Columbus, Ohio 43210, USA*
[5]*School of Physics and Astronomy, University of Leeds, LS2 9JT, United Kingdom*

(Received 27 March 2023; revised 16 July 2023; accepted 25 August 2023; published 2 October 2023)

In magnetic materials with strong spin-lattice coupling, magnon-phonon interactions can change the sensitivity of the lattice thermal conductivity in an applied magnetic field. Applying an out-of-plane magnetic field to change $MnBi_2Te_4$ between antiferromagnetic (AFM), canted antiferromagnetic (CAFM), and ferromagnetic (FM) phases, we controlled the lattice thermal conductivity, generating both a positive and a negative magnetic field dependence. The in-plane thermal conductivity decreases with field in the AFM phase, remains approximately constant in the CAFM phase, and increases with field in the FM phase. We explain this in terms of the field-induced changes of the magnon gap which modifies magnon-phonon scattering. We also report thermal Hall data measured in the same configuration.

DOI: 10.1103/PhysRevB.108.144402

I. INTRODUCTION

The thermal conductivity of a solid has contributions from phonons, electrons, and magnons. The thermal conductivity of the electrons can be modulated in a magnetic field via the Lorentz force, giving rise to magnetoresistance, which is a negative magnetothermal conductivity, or the recently discovered thermal chiral anomaly which gives a positive magnetothermal conductivity [1]. Magnons couple directly to magnetic fields and the thermal conductivity can be altered by the Zeeman effect, red- or blue shifting the magnon dispersion, which alters the thermal occupation of magnon states. Phonons themselves are not generally considered to be directly affected by a magnetic field. However, in magnetic materials with strong spin-lattice coupling, magnon-phonon interactions can thoroughly change that picture. Understanding these interactions can open ways to control the lattice thermal conductivity in active thermal devices (e.g., heat switches) with a magnetic field.

$MnBi_2Te_4$, a magnetic topological insulator, crystallizes in the space group $R\bar{3}m$. It consists of septuple van der Waals layers of Te-Bi-Te-Mn-Te-Bi-Te. This creates a structure that integrates a central layer of MnTe octahedra inside the Bi_2Te_3 archetype, making it a magnetic relative of the 3D topological insulator Bi_2Te_3. $MnBi_2Te_4$ has an *A*-type antiferromagnetic (AFM) structure: the Mn^{2+} spins have moments that are aligned in the out-of-plane direction, are ferromagnetically coupled within each layer, but are weakly antiferromagnetically coupled with neighboring layers. The Néel temperature is $T_N = 25$ K [2]. In an out-of-plane magnetic field with temperatures below T_N, the bulk magnetic ordering undergoes a spin-flop transition followed by a canted AFM (CAFM) ordering. Further increasing the field leads to a phase where the spins in all layers align, making $MnBi_2Te_4$ appear ferromagnetic (FM) at high field [2,3] [depicted in Fig. 1(a)]. Theory predicts that interplay between the magnetic structure and the topologically nontrivial bands produces rich topological phase transitions in an applied magnetic field [4–7]. Raman spectroscopy studies in $MnBi_2Te_4$ show strong coupling between spin and lattice. In these studies, certain A_{1g} optical phonon modes have peak intensity strongly affected by the magnetic ordering [8,9]. Therefore, we expect magnetic ordering transitions in $MnBi_2Te_4$ to exhibit nonmonotonic magnetoelectrothermal transport phenomena.

In this study we measure the in-plane thermal conductivity (κ_{xx}) of AFM-$MnBi_2Te_4$ from 2 to 30 K in an out-of-plane magnetic field. Characteristic changes in κ_{xx} coincide with the boundaries of the field-induced magnetic phase transitions in this material. κ_{xx} decreases with field in the AFM phase, has relatively small field dependence in the canted phase, and increases again with field in the FM phase [Fig. 1(a)]. The measured data agree with reported thermal transport data in literature [10,11]. The magnitude and sign of the changes cannot be explained by either the magnon thermal conductivity or the electronic thermal conductivity. We interpret our results in terms of a magnon-number nonconserving magnon-phonon confluence interaction process. We propose that the magnon gap plays a crucial role in controlling the phase space of energy momentum that allows magnon-phonon scattering [12], suggesting that two-magnon to one-phonon scattering is the dominant spin and lattice interaction in $MnBi_2Te_4$. Theoretical and experimental studies have suggested a thermal Hall effect originating from magnon-phonon interactions [13–20]. We also report thermal Hall data measured in the same configuration. Our measured thermal Hall signal is dominated by

*heremans.1@osu.edu

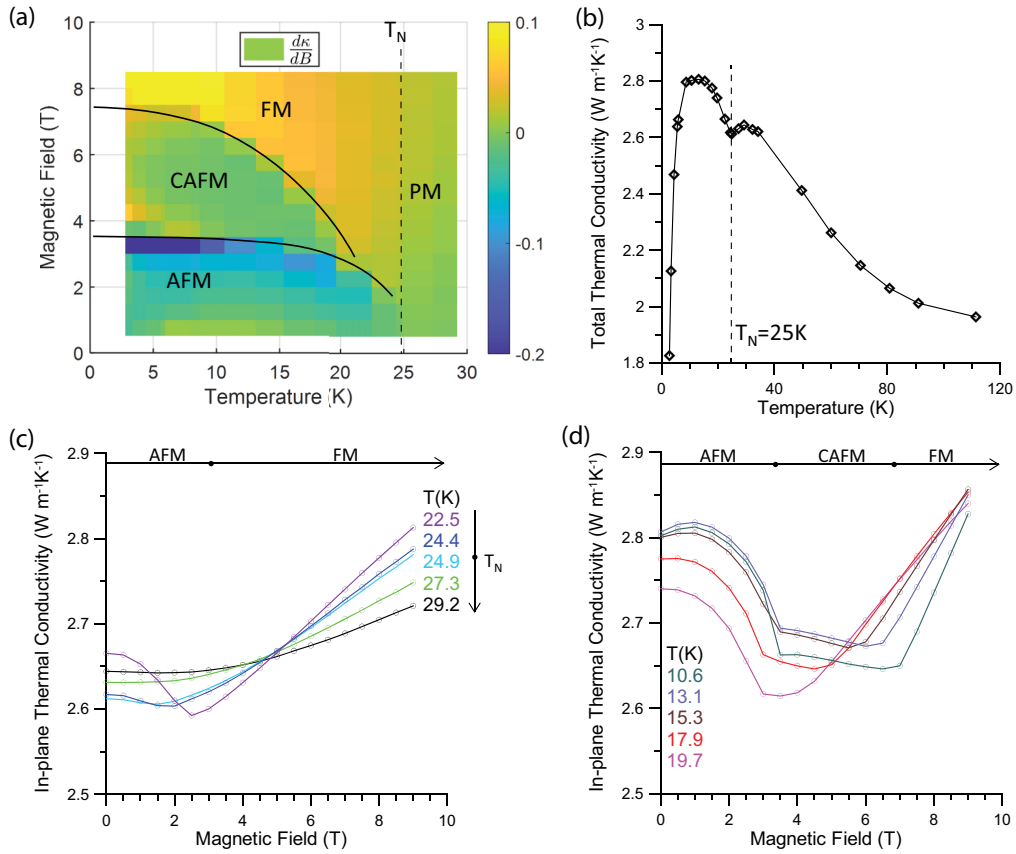

FIG. 1. (a) Magnetic ordering phase diagram, full lines from the literature [2,3]. Color map is reconstructed by taking field derivatives $d\kappa_{xx}/dB$ of following frames. Large negative value near boundary of AFM phase corresponds to spin-flop transition. (b) Temperature dependence of total in-plane thermal conductivity κ_{xx}. κ_{xx} decreases at ordering temperature $T_N = 24.5$ K indicating scattering of phonon to magnon. (c), (d) Field dependence of in-plane thermal conductivity $\kappa_{xx}(B_z)$. Across ordering temperature, $\kappa_{xx}(B_z)$ develops contrasting behavior at different field ranges. Above T_N, κ_{xx} plateaus at low field, then slightly increases with field. Below T_N, κ_{xx} decreases with field at low field and increases linearly in field at high field. Magnetic field at which field dependence changes corresponds to transition from AFM to FM ordering. Below 20 K, in addition to initial decrease in AFM phase and linear increase in FM phase, there is plateau in magnetic field range corresponding to canted AFM ordering phase.

electronic thermal Hall contributions, which show an anomalous thermal Hall effect at the spin-flop transition, which strongly resembles the electrical Hall data. The magnitude of the thermal Hall signal is close to an estimation using the Wiedemann-Franz law. The result points toward an electronic origin of thermal Hall signal and shows no evidence for a thermal Hall signal originated from magnon-phonon interaction.

A. In-plane thermal conductivity in an out-of-plane magnetic field

Single crystals of $MnBi_2Te_4$ were grown by adapting the previously established flux method [21] by slow cooling Bi_2Te_3 and MnTe powders in approximately a 5:1 ratio into an alumina Canfield crucible and centrifuging at 595 °C. Crystals with lengths and widths of 3–8 mm and thicknesses of 10–200 μm were prepared for transport measurements. Hall effect characterization of the carrier concentration (see Supplemental Material [22]) of the samples shows that electrons are the majority charge carriers. The electron concentration at 20 K is from 6×10^{19} to 1×10^{20} cm^{-3}. This is very similar to other values reported, typically ranging from 7×10^{19} to 1×10^{20} cm^{-3} [23,24]. The carrier concentration indicates that the Fermi level is about 0.3 eV into the conduction band [4]. The *n*-type defects responsible for doping were explored by Hou *et al.* and Du *et al.* both experimentally and computationally [25,26]. $MnBi_2Te_4$ growth faces challenges with donor $Bi_{Mn}+$ antisite defects [23,27], which heavily *n*-type dope the crystal.

Figure 1(b) shows the temperature dependence of the in-plane thermal conductivity κ_{xx} without applied magnetic field. This agrees with data previously reported in the literature [10,21]. The electronic thermal conductivity was reported to follow a T^1 law [21], and can be estimated from the resistivity of the sample using the Wiedemann-Franz law with the free-electron Lorenz ratio to be of the order of 0.2 W m^{-1} K^{-1} at 100 K. It is generally much smaller than the total κ_{xx}. At temperatures slightly above 30 K, which are above the T_N of 24.5 K, the lattice thermal conductivity dominates. Around T_N and below, both the lattice thermal conductivity and the magnon thermal conductivity $\kappa_{\text{lattice}} + \kappa_{\text{magnon}}$ must be considered, while the electronic thermal conductivity diminishes and contributes less than 0.05 W m^{-1} K^{-1} to the total thermal conductivity of 2.62 W m^{-1} K^{-1}. In yttrium iron garnet, κ_{magnon} was estimated to be up to ∼1 W m^{-1} K^{-1} at

2 K and becomes a significant contribution as temperature decreases [28]. If κ_{magnon} were significant in $MnBi_2Te_4$ in this range, we would see an increase of κ_{xx} as the temperature decreases below T_N, yet we observe a clear suppression of κ_{xx} in this temperature range. A similar anomaly in $\kappa_{xx}(T)$ was observed in some other magnetic materials near the ordering temperature [29–31]. Comparing the experimental data above and below the Néel temperature $T_N = 24.5$ K, one notices that $\kappa_{xx}(T)$ below T_N is much smaller compared to what it would be if the data above T_N were simply extrapolated following the $1/T$ law expected for the Umklapp-dominated lattice thermal conductivity. Combined with the observation of a peak in heat capacity at the Néel temperature [32], we conclude that magnons emerge at $T < T_N$ and the magnons do not carry much additional heat but instead induce strong phonon-magnon scattering in the ordered phase.

The field dependence of the in-plane thermal conductivity $\kappa_{xx}(B_z)$ is shown in Figs. 1(c) and 1(d). Note that Fig. 1(c) shows data in the vicinity of T_N, while Fig. 1(d) shows data at lower temperatures. As the temperature decreases towards the ordering temperature, $\kappa_{xx}(B_z)$ develops an interesting field dependence. At 29.2 K, we observe a slight increase in $\kappa_{xx}(B_z)$ with an applied magnetic field up to 9 T. This magnetic field-induced increase in thermal conductivity grows larger as the temperature approaches T_N. Below T_N, 22 K $< T <$ 25 K, κ_{xx} decreases at low field and increases linearly at high field. Far below T_N, $T <$ 22 K, the canted AFM ordering phase appears in the intermediate field region. Our data in Fig. 1(d) show that κ_{xx} saturates in this region with a weak field dependence. In the FM phase, the field dependence becomes a linear increase with field. In Fig. 1(a) we plot the derivative $d\kappa_{xx}/dB_z$ as a function of B_z and T and overlay the known magnetic phase diagram [2,3]. Discontinuities in $d\kappa_{xx}/dB_z$ coincide precisely with the magnetic phase boundaries, indicating that the changes in thermal conductivity are related to the magnetic phases [2,3].

B. Theory for $\kappa_{xx}(B_z)$

The field dependence of the thermal conductivity below T_N is unlikely due to electrons, because they contribute less than 0.05 W m^{-1} K^{-1} to κ_{xx} and the resistivity data show less than a 2% decrease in a 9-T magnetic field at 25 K. Therefore, we must look at phonon and magnon contributions. Above T_N, a high magnetic field polarizes the paramagnet into a forced, more ferromagnetically ordered state; thus, magnetic scattering of phonons is reduced. This explains well the κ_{xx} (B_z) data above T_N.

The κ_{xx} (B_z) trends below T_N can be summarized as follows: A decrease in κ_{xx} (B_z) in the AFM phase that becomes more linear at lower temperature, a sharp drop at the spin-flop transition, a relatively small field dependence in the CAMF phase, and a linear increase with field in the FM phase. Strong suppression of thermal conductivity in a magnetic field in the AFM phase and a sharp drop at the spin-flop transition were also reported in the multiferroic materials [19] and Ni_3TeO_6 [18] although the origin was not well established. A linear increase in thermal conductivity with magnetic field was also reported in $Na_2Co_2TeO_6$ [33] and attributed to a reduction of magnon-phonon scattering. An increase in thermal conductivity at high field was observed in Bi-Sb topological insulators and attributed to the thermal chiral anomaly [1]. This occurs when an applied magnetic field is collinear with the heat flux and parallel to the Weyl-points separation [1]. Although the FM phase of $MnBi_2Te_4$ is predicted to be a type II Weyl semimetal with Weyl-points separation from Γ to Z [7], in our experimental setup the applied heat-flux direction is perpendicular to the Weyl-points separation, ruling out the thermal chiral anomaly. The theory of Fermi arc mediated entropy transport in Weyl semimetals [34] also predicts an increase of thermal conductance that is linear with an applied magnetic field that is perpendicular to the surfaces that host topologically protected Fermi arcs. In our experimental setup, it is possible that a small, unintentional misalignment of the out-of-plane magnetic field exists, so there may be a small in-plane magnetic field component $B_{\text{in-plane}}$ perpendicular to the arcs. However, no change was observed when the $B_{\text{in-plane}}$ component was increased intentionally by setting a small (but intentionally) misaligned angle between the applied magnetic field and the sample's out-of-plane direction (see Supplemental Material), contrary to the theoretical prediction. In our samples, we note that the position of the Fermi level of $MnBi_2Te_4$ is far (0.3 eV) from the bulk gap. Thus, the measured magnetothermal transport behavior is unlikely to be due to topological properties.

To understand the behavior of the $\kappa_{xx}(B_z)$ data below T_N, we calculated the evolution of the magnon bands and inferred the consequences for magnon-phonon interactions. We used atomistic spin dynamics (see Supplemental Materials) based on the Heisenberg model parametrized from inelastic neutron-scattering measurements of $MnBi_2Te_4$ [35]. The Hamiltonian is

$$\begin{aligned}\mathcal{H} = &-\frac{1}{2}\sum_{\langle ij\rangle_\parallel} J_{ij}\mathbf{S}_i\cdot\mathbf{S}_j - \frac{1}{2}\sum_{\langle ij\rangle_\perp}\mathbf{S}_i\cdot\mathbf{S}_j \\ &-\frac{1}{2}\sum_{\langle ij\rangle_\perp} J_c^{\text{aniso}}\mathrm{S}_i^z\mathrm{S}_j^z - D\sum_i\left(\mathrm{S}_i^z\right)^2 \\ &-\sum_i \mu_s\mathbf{B}\cdot\mathbf{S}_i\,, \end{aligned} \tag{1}$$

where i labels the Mn ions, $\mathbf{S}_i$ are unit vectors, J_{ij} are the pairwise intralayer exchange interactions, J_c is the nearest-neighbor interlayer exchange, J_c^{aniso} is the nearest-neighbor interlayer anisotropic two-ion exchange, D is the single-ion uniaxial anisotropy energy, $\mu_s = 5\mu_B$ is the size of the Mn magnetic moment in Bohr magnetons, and $\mathbf{B}$ is the externally applied magnetic field in tesla. The magnon-band dispersions in the ordered magnetic phases are calculated by solving the Landau-Lifshitz-Gilbert equation and calculating the spin-spin correlation functions in frequency and reciprocal space. The values of all parameters and the methods are detailed in the Supplemental Material.

Figure 2 shows the calculated magnon-band dispersions. For reference, the dashed lines qualitatively depict the lowest velocity, in-plane acoustic branch of the phonon dispersion of $MnBi_2Te_4$ based on the monolayer phonon dispersion [5], dispersing from 0 to 5 meV from the zone center to the edge. Our experiment data were measured from 3 to 25 K, corresponding to a k_BT scale of 0.25–2.15 meV.

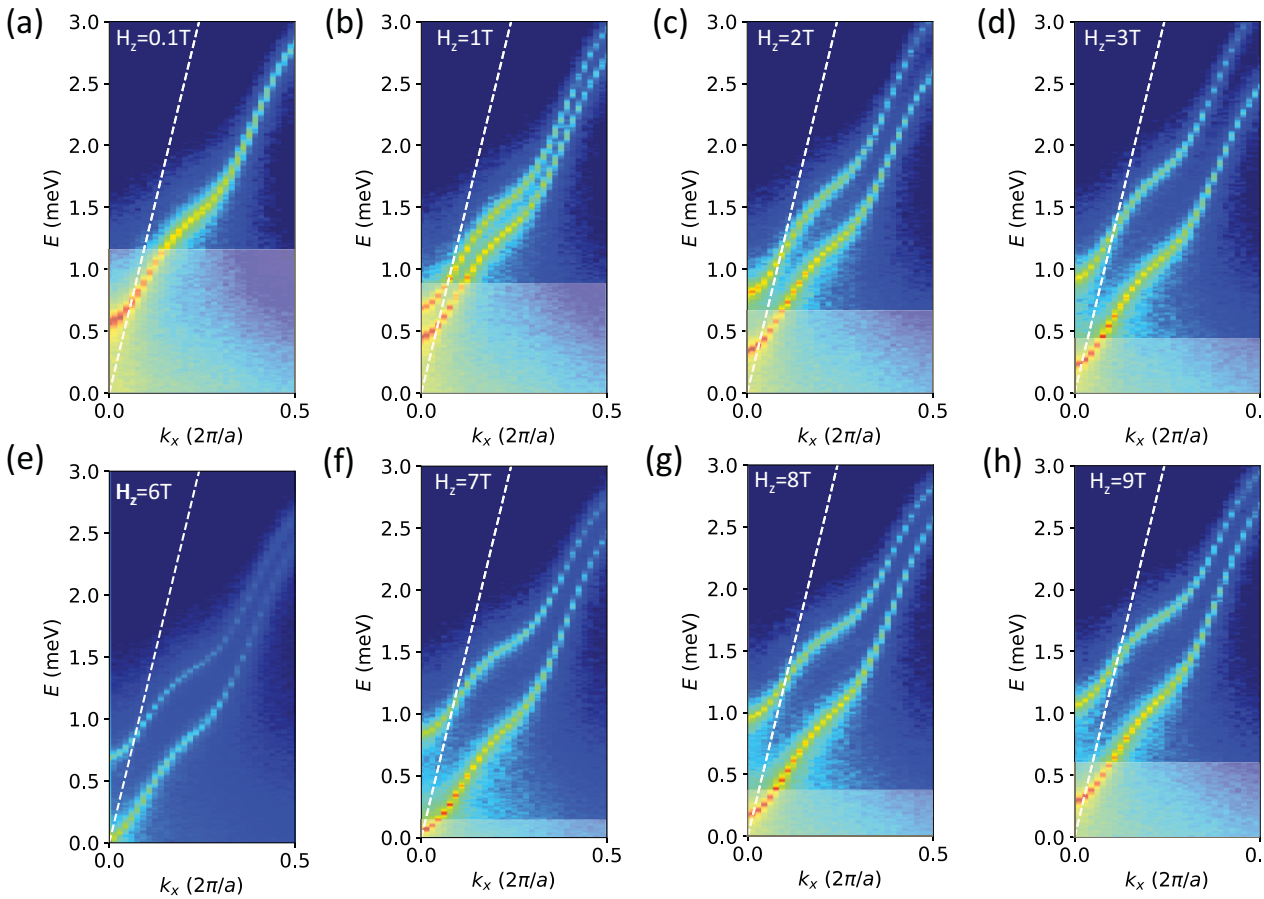

FIG. 2. Calculated magnon band evolution in out-of-plane magnetic field. (a)–(d) magnon bands in AFM ordering phase; (e) magnon bands in canted AFM ordering phase; and (f)–(h) magnon bands in FM ordering phase. Dashed lines qualitatively depict lowest velocity, in-plane longitudinal acoustic branch of phonon dispersion of $MnBi_2Te_4$ based on monolayer phonon dispersion [5]. Light-shaded regions mark forbidden region for magnon-number nonconserving confluence process.

In zero magnetic field, the system is in the AFM phase and the magnons have a near-linear dispersion [Fig. 2(a)]. There are two modes with opposite magnon spin polarization, but in zero field these are degenerate. A 0.6-meV gap at the zone center is induced by the magnetic anisotropy, enhanced by the exchange energy in antiferromagnets. An external magnetic field along z breaks the symmetry between the spin-up and spin-down moments, thus lifting the degeneracy of the AFM magnon branches into two bands with a gap proportional to the external field strength [Figs. 2(b)–2(d)]. Increasing the magnetic field blueshifts one branch and redshifts the other. The redshifted branch becomes the dominant scatterer since the thermal magnon density increases as the band moves to lower energies, whereas the magnon occupation of the high-energy branch decreases. Once the lower magnon mode has closed the energy gap at the zone center, further increasing the applied magnetic field causes an instability in the magnetic order, producing the spin-flop transition and the CAFM phase [Fig. 2(e)]. In the CAFM phase, there is a gapless magnon branch attributed to a Goldstone mode and another high-energy branch. The gapless mode retains its dispersion throughout the CAFM regime without a dependence on the magnetic field. Above a critical field, the magnetic moments are forced to align with the magnetic field, and the FM phase is established with the upper branch being the ferromagnetic-like branch and the lower being of an antiferromagnetic branch with zero magnetization [Figs. 2(f)–2(h)] [36]. The magnetic field increases the energy of both modes, opening a gap in the zone center proportional to the Zeeman energy, $g\mu_B B_z$.

The trends of κ_{xx} (B_z) cannot be explained by magnon thermal conductivity based on the calculated magnon spectrum. The magnon gap closed by the field in the CAFM phase would result in a higher magnon density, thus increasing heat-carrier density. Given the similar dispersion, magnon thermal conductivity would increase in the CAFM phase. This contrasts with the data presented in which κ_{xx} approaches a minimum as the gap is closed, stays at the minimum when the gap is zero throughout CAFM phase, and increases as the gap opens again.

To understand the changes in thermal conductivity in the different magnetic phases we consider the relationship between the magnon spectrum and the acoustic phonon dispersion. To first order, the dominant magnon-phonon interactions can be broken down into three classes: hybridization at crossing points of the dispersion, the magnon-number nonconserving confluence process, and magnon-number conserving Cherenkov scattering [12].

Magnon-phonon hybridization can occur at the touching points between magnon and phonon dispersions. The strength of magnon-phonon hybridization depends on the volume of the phase space at the touching point [13]. In all cases here, the bands simply cross, therefore the hybridization is likely to be weak. In the CAFM phase, there is no magnon gap for the lower branch; thus, hybridization cannot happen on the lower branch, yet the thermal conductivity forms a minimum in this regime, suggesting hybridization is not the dominant mechanism to explain the data. From the neutron-scattering data [35], the hybridization was also not observed, again suggesting that it is a weak effect.

Cherenkov scattering, which conserves the magnon number, can be expected in all magnetic phases. This process involves a magnon scattering into a phonon and a lower-energy magnon. The scattering rate for this process depends on the detailed shape of the magnon dispersion but is allowed by energy and momentum conservation throughout the Brillouin zone. The scattering cross section will have some field dependence as the magnon dispersion changes with field, but no angular momentum is transferred to the lattice and both total energy and total linear momentum of the two magnons and one phonon are conserved; thus, it cannot alter the thermal transport. Finally, we suggest that the magnon-number nonconserving confluence process where both energy and angular momentum are transferred is the most relevant process in explaining our data. In this process, two magnons interact with a phonon. The process must obey the conservation of energy and angular momentum $\epsilon_{\mathbf{k}} + \epsilon_{\mathbf{k}'} - \omega_{\mathbf{q}\lambda} = 0$, where $\epsilon_{\mathbf{k}}$ is a magnon dispersion and $\omega_{\mathbf{q}\lambda}$ is the phonon dispersion with polarization λ. Crucially, *this process is forbidden for phonons at energies less than twice the size of the magnon gap*. These low-energy phonons, corresponding to long wavelengths, typically can travel long distances across the lattice without scattering. They also have a very large thermal population according to Bose-Einstein statistics. Thus, they are the dominant heat-carrying phonons. As the magnon gap closes to zero in the CAFM phase, the confluence process is allowed everywhere in the Brillouin zone and interactions between magnons and the dominant heat-carrying phonons can occur. The zero gap in the CAFM phase also leads to a higher magnon density. In the end, two factors work together to explain the flat and lower thermal conductivity data in the CAFM phase: lower momentum phonons being scattered, and higher magnon density causing more scattering. These two factors have the opposite field dependence in the AFM and FM phases. In the AFM phase, the forbidden region becomes smaller with field, while in the FM phase, the forbidden region expands with field. This explains the opposite field dependence of thermal conductivity in these two phases. In Fig. 1(a), we notice that the magnetic field dependence $d\kappa_{xx}/dB_z$ becomes larger in both AFM and FM phases as the temperature decreases. This behavior can be explained in terms of the smearing of the forbidden gap at finite temperature.

C. Thermal Hall effect

Thermal Hall effect can arise as a result of magnon-phonon interactions in antiferromagnets, as suggested by some theoretical studies. If the magnon-phonon interaction is strong, anticrossing points at magnon-phonon hybridization can generate hotspots of Berry curvature and thermal Hall effect [14]. In an out-of-plane external magnetic field, both antiferromagnets [15] and ferromagnets [16] may have magnon-polaron bands that can carry Chern number, even though the individual magnon and phonon bands are topologically trivial by themselves. This could give rise to a phonon Hall effect. Our magnon band calculation shows there is a possibility that magnon-phonon hybridization can occur in $MnBi_2Te_4$. However, this effect is not seen in neutron-scattering data [35]. The thermal Hall effect, in the form of magnetic field dependence of κ_{xy}, was measured and is shown in Fig. 3(a). Above T_N, κ_{xy} is a linear function of the field up to 9 T with the absolute value of the slope $d\kappa_{xy}/dB_z$ decreasing as the temperature decreases. Below T_N, the absolute value of κ_{xy} shows an abrupt increase at the spin-flop transition with increasing field. κ_{xy} is congruent with the electrical Hall resistivity (see Supplemental Material and Ref. [37]). In Fig. 3(b), we show the calculated $\kappa_{xy,\mathrm{WFL}} = \sigma_{xy}L_0T$ from the Wiedemann Franz law (WFL), where L_0 is the free-electron value of the Lorenz number. $\sigma_{xy}L_0T$ is about half of the measured value for κ_{xy}. Figures 3(c) and 3(d) show raw data points and averaged curves at $T = 10.6$ and 15.3 K, respectively. A drop in κ_{xy} at 3.5 T is observed, coinciding with the spin-flop transition, and we attribute it to the anomalous thermal Hall effect. The close agreement within an order of magnitude indicates that the majority of thermal Hall conductivity is electronic in origin and is from the bulk. However, it is unexpected that the measured κ_{xy} is larger than the estimated value using WFL, i.e., $\kappa_{xy} > \sigma_{xy}L_0T$. If κ_{xy} is purely electronic and the Lorenz number is identical to the free-electron value, κ_{xy} is shorted by the lattice thermal conductivity, and we would expect $\kappa_{xy} < \sigma_{xy}L_0T$. The WFL with the free-electron Lorenz number is something that strictly only holds for elastic diffuse scattering. It is therefore not *a priori* for thermal transport in magnetic field or in the anomalous case of a magnetic material. In this case, it could be attributed to either a doubling of the Lorenz ratio over the free-electron value, or to a magnon contribution, or to a chiral phonon effect either due to skewed magnetic scattering [38] or magnon-polaron bands [13–20]. If there were a phonon Hall effect, it would also be visible at the CAFM to FM, yet we do not see evidence for this. Perhaps the effect is too small compared to the electronic signal. Revisiting the interpretation of the κ_{xy} data and neutron-scattering data [35], we conclude that there is no evidence of magnon-phonon hybridization but the main interaction between magnon and phonon in $MnBi_2Te_4$ is a scattering effect, which we explained, controlled by the magnon band gap.

II. CONCLUSION

In summary, we show that $MnBi_2Te_4$ exhibits a significant and complex field-dependent magnetothermal conductivity. We elucidate the mechanism to be one where phonons carry the heat and are subjected to magnetic scattering. More specifically, the two-magnons scatter, one-phonon process is likely the dominant interaction that affects thermal transport in $MnBi_2Te_4$ in an out-of-plane magnetic field. Magnon-phonon interactions can induce an important field dependence to the amount of heat carried by the lattice, potentially opening a

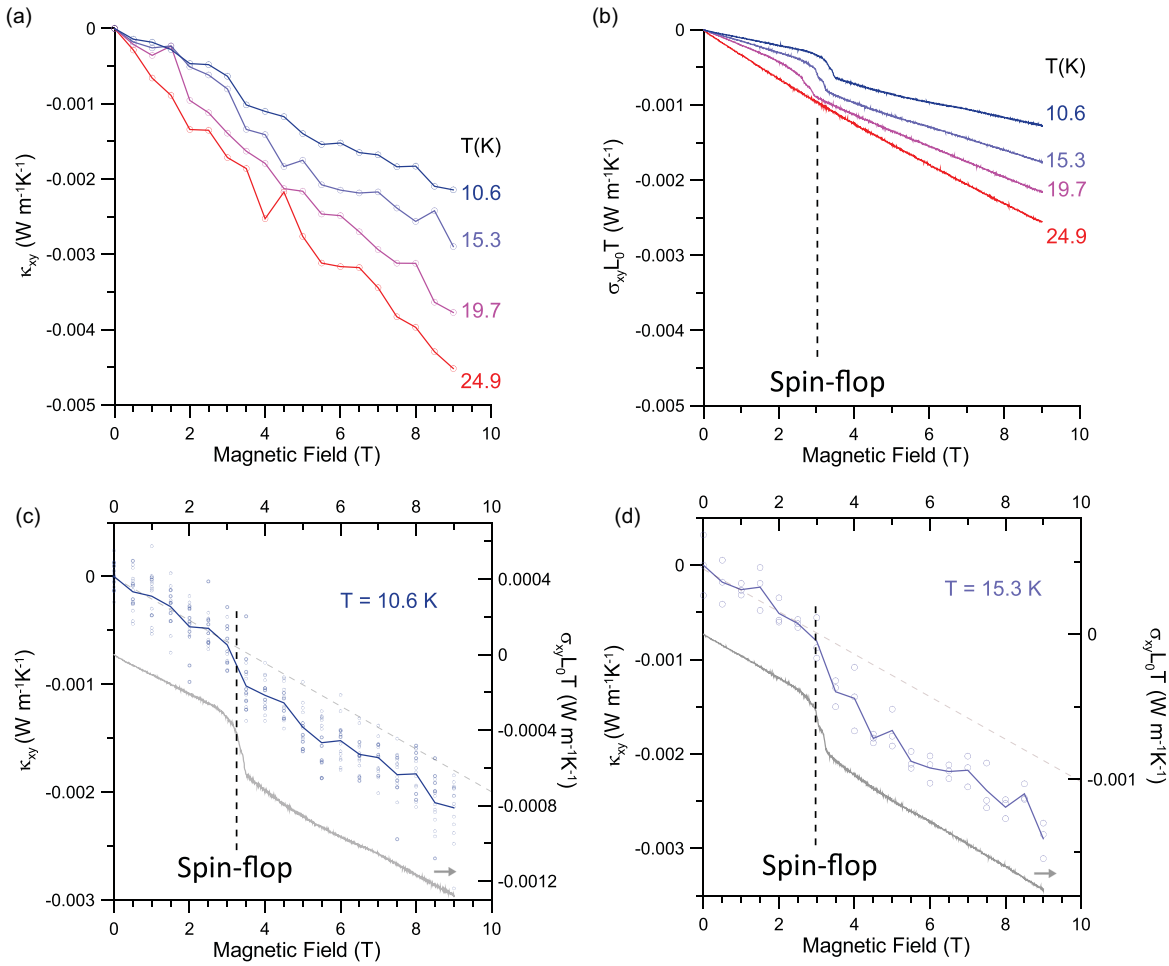

FIG. 3. Thermal Hall conductivity and comparison with Wiedemann-Franz law. (a) Thermal Hall conductivity κ_{xy} vs applied magnetic fields measured below T_N. (b) Thermal Hall conductivity calculated from Wiedemann-Franz law $\kappa_{xy} = \sigma_{xy}L_0T$ at corresponding temperatures. Quantitatively, measured thermal Hall conductivity is approximately twice as large as values predicted by Wiedemann-Franz law. (c), (d) Blown-up plots of κ_{xy} data at 15.3 and 10.6 K show anomalous thermal Hall effect with distinctive jump at spin-flop transition. Individual data points are shown along with lines connecting their mean values at each magnetic field. Dashed lines are linear fit drawn through low field data points in the CAFM phase. Axes on right show corresponding thermal Hall conductivity calculated using WFL and electrical conductivity for comparison.

mechanism to realize heat switches, an enabling technology for solid-state heat engines and controlled cooling technologies.

The datasets generated and/or analyzed during the current study are available from the corresponding author on reasonable request.

ACKNOWLEDGMENTS

We thank Dr. Brian Skinner for the helpful discussions. Simulations in this work were undertaken on ARC4, part of the High Performance Computing facilities at the University of Leeds, U.K. We acknowledge the U.S. Office of Naval Research MURI "Extraordinary electronic switching of thermal transport" Grant No. N00014-21-1–2377 to R.A.N., J.E.G., and J.P.H., support from U.S. Department of Defense SMART Fellowship to B.L.W., U.S. National Science Foundation MRSEC "Center for Emerging Materials," Grant No. DMR 201 1876 to D.D.V., and support from Royal Society University Research Fellowship No. URF/R1/180333 to J.B.

The samples were synthesized by R.A.N. and J.E.G.; the experiments were designed and carried out by D.D.V. and B.L.W. under supervision of J.P.H.; the integration between theory and experiment was done by D.D.V., J.B., and J.P.H., and the magnon spectrum calculations were done by J.B. All authors contributed to data analysis and writing the manuscript.

The authors declare no competing financial interests.

[1] D. Vu, W. Zhang, C. Şahin, M. E. Flatté, N. Trivedi, and J. P. Heremans, Thermal chiral anomaly in the magnetic-field-induced ideal Weyl phase of $Bi_{1-x}Sb_x$, Nat. Mater. **20**, 1525 (2021).

[2] P. M. Sass, J. Kim, D. Vanderbilt, J. Yan, and W. Wu, Robust a-type order and spin-flop transition on the surface of the antiferromagnetic topological insulator $MnBi_2Te_4$, Phys. Rev. Lett. **125**, 037201 (2020).

[3] S.-K. Bac, K. Koller, F. Lux, J. Wang, L. Riney, K. Borisiak, W. Powers, M. Zhukovskyi, T. Orlova, M. Dobrowolska, J. K. Furdyna, N. R. Dilley, L. P. Rokhinson, Y. Mokrousov, R. J. McQueeney, O. Heinonen, X. Liu, and B. A. Assaf, Topological response of the anomalous Hall effect in $MnBi_2Te_4$ due to magnetic canting, npj Quantum Mater. **7**, 46 (2022).

[4] M. M. Otrokov, I. I. Klimovskikh, H. Bentmann, D. Estyunin, A. Zeugner, Z. S. Aliev, S. Gaß, A. U. B. Wolter, A. V. Koroleva, A. M. Shikin *et al.*, Prediction and observation of an antiferromagnetic topological insulator, Nature (London) **576**, 416 (2019).

[5] J. Li, Y. Li, S. Du, Z. Wang, B. L. Gu, S. C. Zhang, K. He, W. Duan, and Y. Xu, Intrinsic magnetic topological insulators in van der Waals layered $MnBi_2Te_4$-family materials, Sci. Adv. **5**, eaaw5685 (2019).

[6] D. Zhang, M. Shi, T. Zhu, D. Xing, H. Zhang, and J. Wang, Topological axion states in the magnetic insulator $MnBi_2Te_4$ with the quantized magnetoelectric effect, Phys. Rev. Lett. **122**, 206401 (2019).

[7] C. Lei, S. Chen, and A. H. MacDonald, Magnetized topological insulator multilayers, Proc. Natl. Acad. Sci. USA **117**, 27224 (2020).

[8] H. Padmanabhan, M. Poore, P. K. Kim, N. Z. Koocher, V. A. Stoica, D. Puggioni, H. Wang, X. Shen, A. H. Reid, M. Gu *et al.*, Interlayer magnetophononic coupling in $MnBi_2Te_4$, Nat. Commun. **13**, 1929 (2022).

[9] J. Choe, D. Lujan, M. Rodriguez-Vega, Z. Ye, A. Leonardo, J. Quan, T. N. Nunley, L. Chang, S. Lee, J. Yan, G. A. Fiete, R. He, and X. Li, Electron-phonon and spin-lattice coupling in atomically thin layers of $MnBi_2Te_4$, Nano Lett. **21**, 6139 (2021).

[10] H. Zhang, C. Q. Xu, S. H. Lee, Z. Q. Mao, and X. Ke, Thermal and thermoelectric properties of an antiferromagnetic topological insulator $MnBi_2Te_4$, Phys. Rev. B **105**, 184411 (2022).

[11] R. A. Robinson, S. H. Lee, L. Min, J. Ning, J. Sun, and Z. Mao, Possible evidence of Weyl fermion enhanced thermal conductivity under magnetic fields in the antiferromagnetic topological insulator $Mn(Bi_{1-x}Sb_x)_2Te_4$, Phys. Rev. B **107**, 235140 (2023).

[12] A. Rückriegel, S. Streib, G. E. W. Bauer, and R. A. Duine, Angular momentum conservation and phonon spin in magnetic insulators, Phys. Rev. B **101**, 104402 (2020).

[13] T. Kikkawa, K. Shen, B. Flebus, R. A. Duine, K. I. Uchida, Z. Qiu, G. E. W. Bauer, and E. Saitoh, Magnon polarons in the spin seebeck effect, Phys. Rev. Lett. **117**, 207203 (2016).

[14] X. Zhang, Y. Zhang, S. Okamoto, and D. Xiao, Thermal Hall effect induced by magnon-phonon interactions, Phys. Rev. Lett. **123**, 167202 (2019).

[15] S. Park and B. J. Yang, Topological magnetoelastic excitations in noncollinear antiferromagnets, Phys. Rev. B **99**, 174435 (2019).

[16] G. Go, S. K. Kim, and K. J. Lee, Topological magnon-phonon hybrid excitations in two-dimensional ferromagnets with tunable Chern numbers, Phys. Rev. Lett. **123**, 237207 (2019).

[17] S. Zhang, G. Go, K. J. Lee, and S. K. Kim, SU(3) topology of magnon-phonon hybridization in 2d antiferromagnets, Phys. Rev. Lett. **124**, 147204 (2020).

[18] H. Yang, X. Xu, J. H. Lee, Y. S. Oh, S. W. Cheong, and J. G. Park, Diagonal and off-diagonal thermal conduction with resonant phonon scattering in Ni_3TeO_6, Phys. Rev. B **106**, 144417 (2022).

[19] T. Ideue, T. Kurumaji, S. Ishiwata, and Y. Tokura, Giant thermal Hall effect in multiferroics, Nat. Mater. **16**, 797 (2017).

[20] H. Katsura, N. Nagaosa, and P. A. Lee, Theory of the thermal Hall effect in quantum magnets, Phys. Rev. Lett. **104**, 066403 (2010).

[21] J. Q. Yan, Q. Zhang, T. Heitmann, Z. Huang, K. Y. Chen, J. G. Cheng, W. Wu, D. Vaknin, B. C. Sales, and R. J. McQueeney, Crystal growth and magnetic structure of $MnBi_2Te_4$, Phys. Rev. Mater. **3**, 064202 (2019).

[22] See Supplemental Material at http://link.aps.org/supplemental/10.1103/PhysRevB.108.144402 for methods used to calculate Fig. 2; resistivity and Hall resistivity data; experimental data for test of presence of Fermi arc; magnetothermal conductivity and thermal Hall conductivity data at temperatures $T \geqslant 50$ K; magnetothermal conductivity data at temperatures $T \leqslant 6$ K; moment vs magnetic field on samples; thermal conductivity and magnetothermal conductivity of second sample; field dependence of the Seebeck and Nernst thermopowers, and field dependence and temperature dependence of the ratio $\kappa xy/\sigma xyTL_0$. The Supplemental Material also contains Refs. [39,40].

[23] J. Q. Yan, S. Okamoto, M. A. McGuire, A. F. May, R. J. McQueeney, and B. C. Sales, Evolution of structural, magnetic, and transport properties in $MnBi_{2-x}Sb_xTe_4$, Phys. Rev. B **100**, 104409 (2019).

[24] B. Chen, F. Fei, D. Zhang, B. Zhang, W. Liu, S. Zhang, P. Wang, B. Wei, Y. Zhang, Z. Zuo *et al.*, Intrinsic magnetic topological insulator phases in the Sb doped $MnBi_2Te_4$ bulks and thin flakes, Nat. Commun. **10**, 4469 (2019).

[25] M. H. Du, J. Yan, V. R. Cooper, and M. Eisenbach, Tuning Fermi levels in intrinsic antiferromagnetic topological insulators $MnBi_2Te_4$ and $MnBi_4Te_7$ by defect engineering and chemical doping, Adv. Funct. Mater. **31**, 2006516 (2021).

[26] F. Hou, Q. Yao, C. Zhou, X. Ma, M. Han, Y. Hao, X. Wu, Y. Zhang, H. Sun, C. Liu, Y. Zhao, Q. Liu, and J. Lin, Te-vacancy-induced surface collapse and reconstruction in antiferromagnetic topological insulator $MnBi_2Te_4$, ACS Nano **14**, 11262 (2020).

[27] J. P. Heremans, R. J. Cava, and N. Samarth, Tetradymites as thermoelectrics and topological insulators, Nat. Rev. Mater. **2**, 17049 (2017).

[28] S. R. Boona and J. P. Heremans, Magnon thermal mean free path in yttrium iron garnet, Phys. Rev. B **90**, 064421 (2014).

[29] G. A. Slack, Thermal conductivity of CaF_2, MnF_2, CoF_2, and ZnF_2 crystals, Phys. Rev. **122**, 1451 (1961).

[30] G. A. Slack and R. Newman, Thermal conductivity of MnO and NiO, Phys. Rev. Lett. **1**, 359 (1958).

[31] C. Kittel, Interaction of spin waves and ultrasonic waves in ferromagnetic crystals, Phys. Rev. **110**, 836 (1958).

[32] A. Zeugner, F. Nietschke, A. U. B. Wolter, S. Gaß, R. C. Vidal, T. R. F. Peixoto, D. Pohl, C. Damm, A. Lubk, R. Hentrich *et al.*, Chemical aspects of the candidate antiferromagnetic topological insulator $MnBi_2Te_4$, Chem. Mater. **31**, 2795 (2019).

[33] X. Hong, M. Gillig, R. Hentrich, W. Yao, V. Kocsis, A. R. Witte, T. Schreiner, D. Baumann, N. Pérez, A. U. B. Wolter, Y. Li, B. Büchner, and C. Hess, Strongly scattered phonon heat transport

of the candidate Kitaev material $Na_2Co_2TeO_6$, Phys. Rev. B **104**, 144426 (2021).

[34] T. M. McCormick, S. J. Watzman, J. P. Heremans, and N. Trivedi, Fermi arc mediated entropy transport in topological semimetals, Phys. Rev. B **97**, 195152 (2018).

[35] B. Li, D. M. Pajerowski, S. X. M. Riberolles, L. Ke, J. Q. Yan, and R. J. McQueeney, Quasi-two-dimensional ferromagnetism and anisotropic interlayer couplings in the magnetic topological insulator $MnBi_2Te_4$, Phys. Rev. B **104**, L220402 (2021).

[36] A. G. Gurevich and G. A. Melkov, Magnetization oscillations and waves, in *Magnetization Oscillations and Waves* (CRC Press, Boca Raton, FL, 1996).

[37] S. H. Lee, Y. Zhu, Y. Wang, L. Miao, T. Pillsbury, H. Yi, S. Kempinger, J. Hu, C. A. Heikes, P. Quarterman, W. Ratcliff, J. A. Borchers, H. Zhang, X. Ke, D. Graf, N. Alem, C.-Z. Chang, N. Samarth, and Z. Mao, Spin scattering and noncollinear spin structure-induced intrinsic anomalous Hall effect in antiferromagnetic topological insulator $MnBi_2Te_4$, Phys. Rev. Res. **1**, 012011(R) (2019).

[38] B. Flebus and A. H. MacDonald, Charged defects and phonon Hall effects in ionic crystals, Phys. Rev. B **105**, L220301 (2022).

[39] J. Barker and G. E. W. Bauer, Semiquantum thermodynamics of complex ferrimagnets, Phys. Rev. B **100**, 140401(R) (2019).

[40] A. V. Savin, Y. A. Kosevich, and A. Cantarero, Semiquantum molecular dynamics simulation of thermal properties and heat transport in low-dimensional nanostructures, Phys. Rev. B **86**, 064305 (2012).